Tumor-Derived miR-378a-3p-Containing Extracellular Vesicles Promote Osteolysis by Activating a Dyrk1a/Nfatc1/Angptl2 Axis for Bone Metastasis

Jialin Wang
state key laboratory of oncogenes and related genes,renji-med x clinical stem cell research center,ren ji hospital,school of medicine,shanghai jiao tong university

Xinxing Du
department of urology,ren ji hospital,school of medicine,shanghai jiao tong university

Xiao Wang
state key laboratory of oncogenes and related genes,renji-med x clinical stem cell research center,ren ji hospital,school of medicine,shanghai jiao tong university

Huixiang Xiao
state key laboratory of oncogenes and related genes renji-med x clinical stem cell research center,ren ji hospital,school of medicine,shanghai jiao tong university

Nan Jing
state key laboratoy of oncogenes and related genes,renji-med x clinical stem cell research center,ren ji hospital,school of medicine,shanghai jiao tong university

Wei Xue
department of urology,ren ji hospital,school of medicine,shanghai jiao tong university

Baijun Dong
department of urology,ren ji hospital,school of medicine,shanghai jiao tong university

Wei-Qiang Gao
state key laboratory of oncogenes and related genes,renji-med x clinical stem cell research cencer,ren ji hospital,school of medicine,shanghai jiao tong university

Yu-Xiang Fang (fyx2003108@sina.com)
State Key Laboratory of Oncogenes and Related Genes, Renji-MedX Clinical Stem Cell Research Center, Ren Ji Hospital, School of Medicine, Shanghai Jiao Tong University

---

Research

Keywords: prostate cancer, bone metastasis, extracellular vesicle, miR-378a-3p, osteolytic progression

Posted Date: July 10th, 2021

DOI: https://doi.org/10.21203/rs.3.rs-687415/v1

Version of Record: A version of this preprint was published at Cancer Letters on November 1st, 2021. See the published version at https://doi.org/10.1016/j.canlet.2021.11.017.

Abstract

Background

The majority of the deaths of prostate cancer (PCa) are caused by progression to bone metastatic PCa. The importance of extracellular vesicles (EVs) in the formation of the pre-metastatic niche has been demonstrated in recent years. However, whether and how tumor-derived EVs interact with bone marrow macrophages (BMMs) to release EV-delivered microRNAs to promote osteolysis and to activate pre-metastatic niche formation for PCa bone metastasis remain unclear.

Methods

Bioinformatics and qRT-PCR analyses were used to screen microRNAs and to identify the elevated expression of miR-378a-3p in both serum-derived EVs from PCa patients and in culture medium-derived EVs from PCa cell lines. Functional assays in vitro and in vivo were performed to investigate the functions of miR-378a-3p during PCa progression. IF staining and Dual-luciferase reporter, co-IP, western blot, RIP and ChIP assays were conducted to reveal the underlying mechanism.

Results

We found that EV-mediated release of miR-378a-3p from tumor cells was upregulated in bone-metastatic PCa which keeps a low intracellular concentration of miR-378a-3p, to promote proliferation and the MAOA-mediated epithelial-to-mesenchymal transition (EMT) in PCa cells. In addition, we demonstrated that the enrichment of miR-378a-3p in tumor derived EVs was induced by overexpression of hnRNPA2B1 as a transfer chaperone. After miR-378a-3p-enriched EVs were taken in by BMMs, elevated intracellular concentration of miR-378a-3p promoted osteolytic progression by targeting the Dyrk1a/Nfatc1 pathway. Mechanistically, inhibition of Dyrk1a by miR-378a-3p improved the nuclear translocation of Nfatc1 to promote expression of the downstream target gene Angptl2. As a feedback, increased secretion of Angptl2 into the tumor environment promoted PCa progression.

Conclusions

Our findings indicate that tumor-derived miR-378a-3p-containing EVs play a significant role in promoting prostate cancer bone metastasis by activating a Dyrk1a/Nfatc1/Angptl2 axis in BMMs to induce osteolytic progression, which implicates that miR-378a-3p may be a potential predictor of metastatic PCa. Moreover, reducing the release of miR-378a-3p-containing EVs or inhibiting the recruitment of miR-378a-3p into tumor-derived EVs might be a potential therapeutic strategy for PCa metastasis.

Background

It has been reported that more than 90% of metastatic prostate cancer (PCa) patients will develop bone metastasis [1], which leads to multiple pathological bone destruction with a poor prognosis. Although an eventually osteoblastic proliferation phenotype is displayed in bone metastatic PCa patients, elevated evidences indicate that osteoclast-induced accelerated bone resorption is a crucial step for PCa bone metastasis [2–4]. Thus screening and identifying tumor derived pro-osteoclastic factors, either extracellular vesicles (EVs)-delivered cargoes or secreted soluble ones, are essential for uncovering the mechanism of establishment of pro-bone metastatic niche and is beneficial for treatment and prevention of PCa bone metastases[5].

Increasing evidences show that cargoes of EVs, such as microRNAs, work as intercellular communication “messengers” [6] and are considered to play a key role in tumor progression as building materials of the pro-metastatic niche[7]. In colorectal cancer, for example, tumor-derived miR-934 enriched EVs were found to be able to induce M2 polarization of macrophage to promote tumor metastasis to liver [8]. However, it is still unclear how microRNAs delivered by tumor-derived EVs regulate the development of osteolytic phenotype for establishment of pro-bone metastatic niche and the release of soluble factors [9] by mature osteoclast as a positive feedback loop for tumor metastasis in PCa.

As miR-378a-3p is one of the upregulated EV-delivered microRNAs shown in our previous work [10], and is shown as a regulator during physiological osteolytic progression[11], we herein decided to determine the possible roles of EV-delivered miR-378a-3p in promotion of PCa metastasis. Our results indicated that miR-378a-3p accelerated osteolysis and upregulated the expression and secretion of soluble factors from osteoclasts to promote tumor cell proliferation and metastasis.

Materials And Methods

Cell lines and cell culture

The human PCa cell lines PC3, DU145, C4-2B, LNCAP and the murine leukemic monocyte macrophage cell line RAW264.7 cells were purchased from the American Type Culture Collection (ATCC, Manassas, USA). Benign prostatic hyperplasia cell line BPH1 was purchased from the Deutsche Sammlung von Mikroorganismen und Zellkulturen (DSMZ, German). PC3, DU145, C42-B, LNCAP and BPH1 cells were cultured in DMEM or RPMI-1640 medium (Thermo Fisher Scientific, MD, USA) containing 10% fetal bovine serum (FBS; Gibco). Raw264.7 was cultured in alpha-MEM (Gibco) with 10% FBS.

Plasmid construction

The firefly luciferase expressional vector phE-luc [12] was employed as a backbone for dual-luciferase report assay. Wide type (WT) and mutant (MUT) sequences of putative microRNA-378a-3p target site(s) on 3’UTR of MAOA and Dyrk1a (named as MAOA-WT,MAOA-MUT, Dyrk1a-T1WT, Dyrk1a-T1MUT, Dyrk1a-T2WT, Dyrk1a-T2MUT, Dyrk1a-T3WT, Dyrk1a-T3MUT, DYRK1A-T1WT, DYRK1A-T1MUT, DYRK1A-T2WT, DYRK1A -T2MUT, DYRK1A -T3WT, DYRK1A -T3MUT, DYRK1A-T4WT, DYRK1A-T4MUT, DYRK1A-T5WT, DYRK1A -T5MUT, DYRK1A -T6WT ,DYRK1A -T6MUT, DYRK1A -T7WT and DYRK1A -T7MUT, respectively)

were synthesized (Sangon Biotech Comp, Shanghai, China) and inserted with the backbone respectively. All the constructions were confirmed by sequencing (Sangon Biotech Comp, Shanghai, China) and then extracted and purified using the EndoFree Mini Plasmid Kit (TIANGEN, Beijing, China) for transfection. Above-described gene sequences were listed in Additional file1: Table S1

Cell transfection and luciferase reporter assays

hnRNPA2B1 siRNA or scrambled siRNA control (Tskingke, Biological Technology, Beijing, China) were transfected with the ribo*FECT*™ CP Transfection Kit (Ribobio, Guangzhou, China) at a final concentration of 100 nM. Expression of related genes was confirmed by qPCR and western bolt. Sequences of siRNA in this study were listed in Additional file1: Table S1

For luciferase reporter assays, 5 X 10^4/well PC3 or Raw264.7 cells in 24-well plates were co-transfected with 200ng luciferase reporter vectors described above, 20 ng Renilla luciferase vector (pRL-CMV; Promega, Madison, WI, USA), and 80ng miRNA-378a-3p mimic or scrambled control (Genomeditech, Shanghai, China) using Lipofectamine 3000 (Invitrogen, USA) according to the manufacturer's instructions. Forty-eight hours after transfection, luciferase activities were measured with the Dual-Luciferase Reporter Assay System (Promega, Madison, WI, USA). Reporter luciferase activity was normalized to the internal control Renilla luciferase activity in all samples. Primers for qPCR were listed in Additional file1: Table S1

Lentiviral vector infection

The lentiviral vectors containing miRNA-378a-3p mimic or miRNA-378a-3p inhibitor, shRNA of MAOA or Dyrk1a, and relevant controls were constructed and packaged into lentivirus respectively by Genomeditech Comp (Shanghai, China).

For infection experiment, 1.5×10^5 PC3 cells, 1×10^6 bone marrow-derived macrophages (BMMs) or RAW264.7 cells were infected with related lentivirus (MOI = 10 for PC3 and MOI = 100 for BMMs or RAW264.7) along with 10 μg/ml polybrene dissolved the culture medium. Culture supernatant was replaced by fresh medium containing 10% FBS 24h after infection. Expression of related genes and microRNAs were confirmed by qPCR and western bolt. Above-described gene sequences were listed in Additional file1: Table S1

Cell proliferation

Cell proliferation was measured by CCK-8 assay kit (Dojindo, Kumamoto, Japan). PC3 cells were cultured in the 96-well plate at an initial density of 2000 cells/well and were incubated with CCK-8 for 2 hrs at 37°C. The absorbance values of CCK8 staining were measured at 450 nm using a BioTek Synergy HT microplate reader.

Apoptosis and Cell Cycle assay

Apoptosis and cell cycle assay were processed with an Annexin V-Alexa Fluor 647/PI Kit (Yeasen, Shanghai, China) and Cell Cycle Analysis Kit (Yeasen, Shanghai, China), according to the manufacturer's

protocol. Briefly, 10^6 cells were collected and dual-incubated with Annexin V- Alexa Fluor 647 and PI for flow cytometry assay. For cell cycle analysis, 10^5 cells per well were seeded in 6-well plate, fixed in 70% ethanol overnight, and stained with PI in staining buffer for 30 min at 37°C. The procedure was protected from light, then collected for flow cytometry assay within 5 hours and analyzed using the flowjo analysis software.

Transwell assay

For transwell assay, 5×10^4 PC3 cells were seeded in the upper chamber (Corning, NY, USA) with 150 μl DMEM Basic Medium, and the lower chamber was loaded with 600 μl DMEM containing 10% FBS. After incubation for 24h, transmigrated cells (on the lower surface of membrane) were fixed with 4% paraformaldehyde for 15 mins, and then stained with 1% crystal violet (Sigma-Aldrich, St. Louis, MO, USA) for 15 mins at room temperature. After that, photograph and cell number count were carried out under a microscope in five random fields.

Induction of osteolysis

BMMs were isolated from the bone marrow of six-week-old male BALB/C mice as previously described [13]. Briefly, Bone marrow cells were collected from tibia and femur to incubate with alpha-MEM supplemented with 10% FBS and 1% penicillin/streptomycin for 48 hours. Non-adherent cells were collected and seeded on 24-well plates at a density of 5.0×10^5 cells/well and incubated in the presence of M-CSF (25 ng/mL, PeproTech, Rocky Hill, NJ, USA) for 48 hours to obtain BMMs. BMMs were further stimulated with M-CSF (25 ng/mL) and RANKL (100 ng/mL, PeproTech) for osteolysis. Culture media were changed every 3 days.

TRAP staining

For TRAP staining, cells were first washed three times with PBS after the culture medium was removed and fixed in 4% paraformaldehyde for 15min, followed by stained using a TRAP staining kit (Nanjing Jiancheng Bioengineering Institute, Nanjing, China) according to the manufacturers' instructions. After 30 min, staining solution was washed off and the TRAP activity was analyzed by colorimetry. At the same time, the number and size of multinucleated (more than three nuclei) osteoclasts were analyzed and calculated by the imageJ software. TRAP staining for paraffin-embedded tissue sections was carried out by Runnerbio biotech. Comp (Shanghai, China) with similar methods. N.Oc/BS (number of osteoclast per bone surface) and ES/BS (eroded surface per bone surface) were used to measure the number and size of osteoclasts in the mouse bone marrow.

RNA isolation and qRT-PCR analysis

Total RNA was extracted using TRIzol (Thermo Fisher Scientific). The EV-delivered microRNA was extracted using the exoRNeasy Mini Kit (Qiagen, German). MicroRNA reverse transcription and qRT-PCR were carried out using Taqman miRNA reverse transcription kit (Thermo Fisher Scientific) and Taqman premix (Takara, Shiga, Japan) respectively. The specific reverse primers and qRT-PCR Taqman probes for miR-378a-3p and snRNA U6 (internal normalization control) were purchased from Thermo Fisher

Scientific. For mRNA expressional analysis, cDNAs were reverse transcribed from 2 μg total RNA with a Prime-Script RT kit (Takara, Shiga, Japan) and amplified with the SYBR-Green Real-time PCR Master Mix (Applied Biosystems, Thermo Fisher Scientific). The mRNA expression level of β-actin was used as an internal normalization control. Comparative quantification was performed by using the 2-ΔΔCt method. All primers are available in the Additional file1: Table S1.

Western blot and co-immunoprecipitation (co-IP)

Nuclear and Cytoplasmic Extraction Reagents (Thermo Fisher Scientific) supplemented with protease inhibitor (Thermo Fisher Scientific) were used to isolate and purify cytoplasmic and nuclear protein in 1×10^7 cultured cells. RIPA (Millipore) supplemented with protease inhibitor and PMSF (Thermo Fisher Scientific) was used to isolate total protein from either cultured cells or clinical tissue samples.

For western blot, after quantified by the Pierce BCA Protein Assay Kit (Thermo Scientific, Waltham, MA, USA), 40 μg of total proteins were separated by SDS-PAGE and transferred to PVDF membrane (Millipore, Bedford, MA, USA). The membrane was blocked with TBST containing 5% BSA at room temperature for 1h and then incubated with the relevant primary antibodies at 4°C overnight, which was then probed by an HRP-conjugated secondary antibody at room temperature for 1h. The relevant proteins were visualized by the ECL (electro-chemiluminescence) detection instrument (Thermo Fisher Scientific) plus HRP substrates.

For co-IP, whole cell lysates were prepared using a lysis buffer containing 50 mM Tris (pH 7.5), 120 mM NaCl, 0.5% NP-40, 5 mM EDTA and protease and phosphatase inhibitors (Thermo Fisher Scientific). Total protein (100 μg) was incubated with 5μg specific antibodies and 20 μl protein G-sepharose beads (Thermo Fisher Scientific) on shaker at 4°C overnight. After washed by Chilled PBS for 4 times (5mins each), the beads-antibody complex was boiled for 10 min to obtain protein supernatant captured by the protein G-sepharose beads for western blot. β-actin was used as a control for input. Information for all antibodies is available in Additional file1: Table S2.

EVs isolation and characterization

DMEM medium with 10% EV-depleted FBS (Thermo Fisher Scientific) was used for cell culture before isolation EVs from culture medium. After using a gradient centrifugation (300x*g* for 10 min, 2000x*g* for 10 min and 10000x*g* for 40min), the supernatant was filtered using a 0.22μm PVDF filter (Millipore, USA) and followed by the ultracentrifugation at 10,0000g for 90min to harvest EVs deposition. EVs were resuspended in PBS to determine EVs size distribution, concentration and morphology by nanosight tracing assay, western blot assay and transmission electron microscopy (TEM) respectively, which was described in our previous work[10], according to Minimal Information 2018 for Studies of Extracellular Vesicles (MISEV2018) guidelines[14].

EVs labelling and tracking

Purified EVs were labeled with the lipophilic membrane dye PKH67 (Sigma, USA) according to the manufacturer's instruction. Labeled EVs were washed with PBS and centrifuged again at 10000×g for 70

min at 4°C for incubation with BMMs (5×10^4 cells per well in a 24-well plate at a concentration of 25μg/mL for 24 h).

For EVs education experiments in vivo, 100 μg/kg EVs were inoculated in mice through tail intravenous injection every other day for 3 weeks. For EV-tracking experiments in vivo, 10μg/kg purified and PKH67 labeled EVs were injected 24h before tissue collection.

Chromatin immunoprecipitation (ChIP) assays

The cell extraction was prepared and the experiment was performed according to manufacturers' instructions by using a ChIP assay kit (Cell Signaling Technology, Danvers, MA, USA). Briefly, ChIP assays were performed using anti-NFATC1 antibody (Santa Cruz Biotechnology, USA) or IgG (Cell Signaling Technology, USA) as a control. After extraction of ChIP DNA, specific fragments (less than 200 bp) containing potential binding sites or control sites were amplified and analyzed by qPCR and sequencing. NFATC1 relative enrichment was calculated by the formula provided in the protocol. Primers used for ChIP assay are available in Additional file1: Table S1.

RNA immunoprecipitation (RIP) assay

RIP assays were performed using a Magna RIP RNA-Binding Protein Immunoprecipitation kit (Millipore, USA). Briefly, cells and EVs were collected and lysed in chilled lysis buffer supplemented with protease inhibitors and RNase inhibitors. Lysates were centrifuged at 14,000×g for 10 min to harvest supernatant for RIP and input (10% volume). The supernatant was incubated with 3 μg anti-hnRNPA2B1 antibody (abcam, England) or IgG (Cell Signaling Technology, USA) in RIP Buffer along with 30 μL A/G protein magnetic beads on rotating overnight at 4°C. Then, the magnetic beads were washed five times, and coimmunoprecipitated miRNAs were extracted using standard RNA isolation method mentioned above. The isolated miRNA was reverse transcribed and then analyzed by qRT-PCR. In addition, miR-378a-3p fold enrichment in immunoprecipitated samples is presented as percent input and compared with IgG isotypic control.

Intratibial injection

Six-week-old male BALB/C athymic nude mice (SLAC, Shanghai, China) were housed and manipulated according to the protocols approved by the Renji Hospital Medical Experimental Animal Care Commission. To establish a bone metastasis model, 2×10^5 PC3-con and PC3-378OE cells were injected intratibially into nude mice, respectively, with treatment of GW4869 (2mg/kg, sigma) intraperitoneally injected every 2 days. Five weeks later, mice were sacrificed and tibiae were collected and fixed in 4% formaldehyde for H&E, IHC(Immunohistochemical) staining and high-resolution microCT(Inveon, Siemens, Germany) to evaluate bone destruction. For high-resolution microCT, the average bone volume/total volume (BV/TV) values and bone mineral density (BMD) of the same tibial lesion areas in each group were analyzed.

Immunofluorescent (IF) staining

Cells were seeded on cover slides placed in 24-well plate and cultured in DMEM medium supplemented with 10% FBS and maintained at 5% CO2 at 37°C for 48 h. Adherent cells on cover slides were fixed with 4% paraformaldehyde for 15mins at room temperature. Cells were permeabilized with 0.3% Triton X-100 and then blocked with 10% normal donkey serum (GeneTex, Irvine, California, USA) for 1 hour at room temperature. After incubated with relevant primary antibody (1:200, diluted in PBS with 1% normal donkey serum) at 4°C overnight, cells were first washed with PBS buffer three times (10mins each) and in turn incubated in dark with Alexa Fluor-594 or Alexa Fluor-488 conjugated secondary antibody (Thermo Fisher Scientific) at room temperature for 1 h. Cells were washed with PBS three times again before mounted with DAPI (Thermo Fisher Scientific). Images of IF staining were observed and photographed by a microscope (Leica DFC420C). All antibodies are available in Additional file1: Table S2.

H&E staining and Immunohistochemical (IHC) staining

H&E staining and Immunohistochemical (IHC) staining for paraffin-embedded tissue sections were carried out by Runnerbio biotech. Comp (Shanghai, China). Tissues were fixed in 4% paraformaldehyde overnight and embedded in paraffin. Paraffin-embedded tissue sections were dewaxed in xylene for 5mins and then hydrated in 100, 95, 85 and 70% ethanol successively. After inactivating endogenous peroxidase in disodium-hydrogen phosphate-2-hydrate, these sections were blocked in 10% donkey serum for 1h at room temperature for IHC staining. After serum blocking, sections were incubated with primary antibody (1:200) at 4°C overnight. After washed with PBS for three times (10 min each), sections were incubated with horseradish peroxidase-conjugated secondary antibody (Vector, Burlingame, CA, USA) for 1 h at room temperature. Sections were then washed with PBS again for three times and were visualized with DAB (Sangon Biotech, Shanghai, China) staining and hematoxylin counterstaining (Beyotime, Shanghai, China). Images were acquired under a microscope (Leica DFC420C) in the same exposure conditions. The effectiveness and specificity of primary antibodies were checked before IHC staining by no-primary antibody control assay. All antibodies are available in Additional file1: Table S2.

Clinical samples

The investigation has been conducted in accordance with the ethical standards and according to the Declaration of Helsinki, national and international guidelines as well as the Committee for Ethical Review of Research Involving Human Subjects at Ren Ji Hospital. Human PCa tissue samples for western blot assay and IHC staining, paired adjacent normal tissue samples for western blot assay and non-paired benign mammary hyperplastic samples for IHC staining were obtained from department of urology, Ren Ji Hospital (Shanghai, China). Written informed consents were obtained from all patients for the application of the specimens used in the study. All clinical data of patients participated in the study were summarized in Additional file 1: Table S3.

Statistical analysis

Data were expressed as mean ± SEM from triplicate experiments. Group differences were analyzed using independent Student's t-test or analysis of variance (ANOVA). Genes differentially expressed between the test and control groups in the GEO datasets (http://www.ncbi.nlm.nih.gov/geo/) were identified using the

Limma R package[15]. And we download the TCGA-PRAD datasets from the TCGA RNA-seq database (https://xena.ucsc.edu/public/), the R package “survival” was used to evaluate the association of all candidate genes with overall survival (OS), disease free survival (DFS), disease free interval (DFI), and progress free interval (PFI) [16]. Results were considered as statistically significant when $p < 0.05$.

Results

EV-mediated release of miR-378a-3p is upregulated in bone-metastatic prostate cancer

In our previous work [10], miR-378a-3p was found as one of the upregulated serum EV-delivered microRNAs in bone-metastatic PCa patients. Besides its function on physiological osteolytic progression[11], we herein wondered whether miR-378a-3p was also involved in regulation of pathological osteolytic progression during PCa bone metastasis. To this end, we first re-examined expression of serum EV-delivered miR-378a-3p by both dataset analysis in GEO database and qRT-PCR assay in clinical samples. As expected, we observed a significantly upregulated expression of serum EV-delivered miR-378a-3p in bone-metastatic PCa (bmPCa) patients (Fig. 1A, 1B and Additional file1: Table S3). On the other hand, miR-378a-3p expression in tissue samples was significantly downregulated in bmPCa tissues group, which indicated an increased release of miR-378a-3p-containing EVs from bmPCa (Fig. 1C). Consistently, data analysis of both GEO database and The Cancer Genome Atlas (TCGA) database from UALCAN (http://ualcan.path.uab.edu)[17] also revealed a lower expression level of miR-378a-3p in metastatic PCa tissues and a negative association with the Gleason Score (Fig. 1D, 1E and Additional file 2: Fig. S1A). Additionally, Kaplan–Meier survival analysis also showed that patients with lower miR-378a-3p expression levels in tumor tissues had both the poorer disease-free interval (DFI) and the poorer progression-free interval (PFI) rate (both $p < 0.01$, Fig. 1F and Additional file 2: Fig. S1B).

Next, we measured expression level of intracellular mature miR-378a-3p and its precursor pri-miR-378a-3p in human BPH-1 cell line and PCa cell lines as well as expression of EV-delivered miR-378a-3p from related culture medium. Consistent with the above findings, the intracellular expression of mature miR-378a-3p was downregulated in PCa cell lines, especially in PC3 cells ($p < 0.0001$), although the expression of its precursor pri-miR-378a-3p was similar among these cell lines. Conversely, the expression of miR-378a-3p was significantly upregulated in medium-derived EVs of PC3 cells (Fig. 1G). Moreover, after treated with an EV release inhibitor GW4869 (10μg/ml, sigma), we observed a significant increase in intracellular concentration of miR-378-3p in PC3 cells along with the repression of EV-miR-378-3p (Additional file 2: Fig. S1C). Taken together, these results implicated that EV-mediated release of miR-378a-3p is upregulated in bone-metastatic PCa, which resulted in a low intracellular concentration in tumor cells.

Overexpression of miR-378a-3p along with repression of EVs release inhibits proliferation and migration of PCa cells in vitro and intratibial tumor growth in vivo.

In order to investigate the regulatory effect of miR-378a-3p on PCa cells, we construct a miR-378a-3p overexpression subclone cell line and a miR-378a-3p inhibitory subclone cell line in PC3 cells respectively (named PC3-378OE vs. PC3-con cell as a control and PC3-anti378 vs. PC3-anti-con as a control respectively, Additional file 3: Fig. S2A). Furthermore, to maintain a high intracellular concentration of miR-378a-3p, we treated PC3-378OE and PC3-con cells with GW4869 for functional assays in vitro. As expected, overexpression of miR-378a-3p along with repression of EVs release significantly increased the intracellular concentration of mature miR-378a-3p compared to either miR-378a-3p overexpression alone or GW4869 treatment alone, and inhibited cell proliferation by CCK8 and Ki67 staining assays (Fig. 2A, 2B and Additional file 3: Fig. S2A). Consistently, antagonists of miR-378a-3p function promoted proliferation of PC3 cells (Additional file 3: Fig. S2B and S2C). Additionally, cell migration was impaired and cell apoptosis was improved in PC3-378OE cells with GW4869, and a converse phenotype was observed when miR-378a-3p was blocked in PC3-anti378 vs. PC3-anti-con cells (Fig. 2C, 2D, Additional file 3: Fig. S2D and S2E).

For in vivo assay, PC3-378OE or PC3-con cells were injected intratibially into nude mice with the treatment of GW4869 (2mg/kg) every 2 days. Five weeks after inoculation, we observed that the tumor growth was attenuated in PC3-378OE group under the condition of EVs release blockage, evidenced by a relatively smaller tumor size and relatively light lesser destruction of trabecular bone structure in the tibia (Fig. 2E). Furthermore, we found that the average BV/TV was significantly upregulated in PC3-378OE group by high-resolution microCT assay (Fig. 2F). Taken together, all these results indicated that overexpression of miR-378a-3p along with blockage of EVs release effectively inhibits proliferation and bone metastasis *in vitro* and *in vivo.*

Overexpression of miR-378a-3p inhibits epithelial-to-mesenchymal transition (EMT) for metastasis by targeting MAOA

In order to investigate potential mechanisms, an online tool (http://www.microrna.org) was utilized to predict possible miR-378a-3p target genes which might contribute to the proliferation and metastasis of PCa cells. The result indicated that MAOA (monoamine oxidase A), a well-known enzyme for regulation of proliferation and metastasis in multiple cancers [18], might be a potential target of miR-378a-3p (Fig. 3A). Co-expression interaction analysis (http://starbase.sysu.edu.cn)[19] using data from TCGA database also indicated a negative association of miR-378a-3p expression with MAOA expression (Fig. 3B). By dual-luciferase reporter assay as a further support, we found that the luciferase activity was significantly inhibited only when we co-transfected a miR-378a-3p mimic with a luciferase reporter vector which contained a wild-type miR-378a-3p binding site sequence (WT) but not a mutant sequence (MT) of MAOA

mRNA 3' untranslated region (UTR) in PC3 cells (Fig. 3C). Also both mRNA and protein expression of MAOA was significantly repressed in PC3-378OE cells treated with GW4869, which revealed that MAOA was a direct target of miR-378a-3p in PCa cells (Additional file 4: Fig. S3A). Furthermore, we herein checked MAOA expression in clinical samples and observed the upregulation of both MAOA mRNA and protein in PCa tissues (Fig. 3D), which was consistent with the data from TCGA database (Fig. 3E and Additional file 4: Fig. S3B). Importantly, the expression of MAOA was further improved in bmPCa tissues, which was consistent with the data from GEO database (Fig. 3F, 3G and Additional file 4: Fig. S3C). On the other hand, by transwell assay, we found that stable knockdown of MAOA in PC3 cells significantly inhibited cell migration in vitro, which displayed a similar effect to that of overexpression of miR-378a-3p in PC3 cells (Fig. 2C, Additional file 4: Fig. S3D and S3E).

Given the fact that MAOA was reported as a key regulator of epithelial-to-mesenchymal transition (EMT) in multiple cancers [20], we herein also wondered whether PCa bone metastasis could be inhibited by targeting MAOA induced EMT. By detection of the expression of EMT markers, we found that in PC3-378OE cells treated with GW4869, the expression of E-cad was significantly upregulated along with a significant downregulation of N-cad and vimintin expression (Fig. 3H and 3I). Consistently, stable knockdown of MAOA exhibited a similar result (Additional file 4: Fig. S3F). Thus, combined these results with our above findings, overexpression of miR-378a-3p along with blockage of EVs release could inhibit PCa bone metastasis by targeting MAOA-mediated EMT.

Overexpression of hnRNPA2B1 leads to enrichment of miR-378a-3p in tumor released EVs

Next, we investigate the potential mechanism regarding enrichment of miR-378a-3p in tumor derived EVs for maintaining its low intracellular concentration. First, we checked and observed no significant difference of EV characteristics derived from BPH-1 and PC3 cells respectively by nanosight tracking assay (NTA), western blot assay and transmission electron microscopy (TEM), which indicated that upregulation of mature miR-378a-3p concentration in tumor derived EVs was not caused by an increased EV release but rather by an enrichment of mature miR-378a-3p in EVs (Additional file 5: Fig. S4A-S4C). It has been reported that hnRNP family played an important role in enrichment of microRNAs in EVs [21]. To determine whether hnRNP family members mediated miR-378a-3p enrichment in EVs, we paid attention to a reported binding motif of hnRNPA2B1, GGAG [22], which harbored in the mature miR-378a-3p, indicating that hnRNPA2B1 might be involved in the EVs-targeted enrichment of miR-378a-3p. For validation, we carried out a RNA immunoprecipitation (RIP) assay and found that miR-378a-3p was significantly enriched in both PC3 cells and PC3-derived EVs (Fig. 4A). Additionally, hnRNPA2B1 protein was significantly enriched in PC3-derived EVs, suggesting a co-enrichment with miR-378a-3p in tumor derived EVs (Fig. 1G and Additional file 5: Fig. S4D). Furthermore, after repressing hnRNPA2B1 expression (Additional file 5: Fig. S4E), the enrichment of mature miR-378a-3p in PC3-derived EVs was significantly attenuated but the intracellular concentration of mature miR-378a-3p was enhanced, which indicated an hnRNPA2B1 mediated miR-378a-3p translocation from cells to EVs (Fig. 4B). Consistent with the oncogenic function of hnRNPA2B1 on EV-enrichment of miR-378a-3p, expression of hnRNPA2B1 was

found to be significantly upregulated in PCa tissues both by analysis of the dataset in TCGA database and by qRT-PCR and western blot assays in clinical PCa and BPH tissue samples (Fig. 4C, 4D, Additional file 5: S4F and Additional file1: Table S3). Also PCa patients with higher hnRNPA2B1 expression exhibited a poorer overall survival (OS) rate as well as a poorer disease free survival (DFS) rate (both $p < 0.01$, Fig. 4E). Collectively, these findings indicated that enrichment of miR-378a-3p in PCa-derived EVs was mediated by overexpression of hnRNPA2B1.

EV-delivered miR-378a-3p promotes osteolytic progression for bone metastasis of PCa via targeting Dyrk1a/Nfatc1 signaling pathway in BMMs.

Given the fact that osteolysis might be an initial process of bone metastasis in malignant tumors [23], we herein wondered whether PCa-derived EVs could be taken in by osteoclasts and/or their precursors (i.e. bone marrow macrophages, BMMs) as potential recipient cells to promote osteolysis for PCa bone metastasis. To this end, we extracted miR-378a-3p–enriched EVs (named 378EVs) from PC3-378OE cells when cultured without GW4869 and EVs from PC3-con cells as controls (named conEVs). By NTA, western blot assay and TEM, we confirmed no significant difference between 378EVs and conEVs (Additional file 6: Fig. S5A-S5C). After labeled with PKH67, a lipid membrane dye, 378EVs or conEVs were incubated with BMMs respectively and we observed that the intake of either 378EVs or conEVs to BMMs was not significantly different in vitro (Fig. 5A). In addition, we transiently transfected PC3-378OE or control cells with Cy3-tagged miR-378a-3p mimics as a tracing marker and again extracted relevant EVs to incubate with BMMs. We observed a significant increased Cy3-miR-378a-3p intake without increase of endogenous pri-miR-378a-3p in BMMs after incubation with 378EVs, supporting the notion that increased intracellular concentration of miR-378a-3p in BMMs was exactly caused by the intake of miR-378a-3p enriched EVs (Fig. 5B and Additional file 6: Fig. S5D). On the other hand, we directly overexpressed miR-378a-3p or control mimics by lentivirus infection in BMMs (Additional file 6: Fig. S5E) and observed a similar phnotype with incubation of 378EVs that the expression of osteolytic markers was significantly upregulated and TRAP-positive cell number as well as osteolytic size were significantly increased in BMMs (Fig. 5C, 5D, Additional file 6: Fig. S5F and S5G). For in vivo assay, we educated nude mice with 378EVs or conEVs (each 100 μg/kg, tail intravenous injection every other day for 3 weeks) before inoculating tumor cells. We observed a significant upregulation of both ES/BS value (Eroded surface/bone surface) and NOc/BS value (number of osteoclast / bone surface) as an evidence of promotion of osteolysis and establishment of pro-metastasis niche (Additional file 6: Fig. S5H). In order to prevent tumor cells from interfering with the already formed niches by secreting miR-378a-3p-enriched EVs during tumor growth, we employed PC3-anti378 cells for inoculation so that no miR-378a-3p enriched EVs would be released. As expected, we observed a more serious osteolysis after education of 378EVs with decreased BV/TV value and bone mineral density (BMD) by microCT scanning and increased osteoclast numbers and bone erosions by TRAP staining assay (Fig. 5E and 5F). Elevated tumor burden was also observed in the bone in 378EVs education group (Fig. 5G). Taken together, all these findings

indicated that intake of miR-378a-3p in BMMs promoted osteolysis to form a pro-metastatic niche for PCa bone metastasis.

To explore the potential mechanism, we attempted to screen and identify potential targets of miR-378a-3p in BMMs. Combined bioinformatics assays on potential target genes of both mmu-miR-378a-3p and hsa-miR-378a-3p with dual-luciferase reporter assay, we revealed that Dyrk1a (dual specificity tyrosine phosphorylation regulated kinase 1A) was a possible target gene of miR-378a-3p, which indicated that highly homologous regulation of downstream by miR-378a-3p occurred in both species and also indicated that related phenotype observed in the mouse could be reconstituted in human (Fig. 6A, 6B, Additional file 7: Fig. S6A and S6B). As expected, after incubation of 378EVs or overexpression of miR-378a-3p with RAW264.7 cells, both mRNA and protein expression of Dyrk1a was repressed (Fig. 6C and Additional file 7: Fig. S6C). Because Dyrk1a has been reported as an osteolytic related gene[24], we implicated that miR-378a-3p promoted osteolysis via targeting Dyrk1a. As a further confirmation, we inhibited Dyrk1a expression or blocked its function by inhibitor harmine (20μg/ml) and found that either treatment upregulated the expression of osteolytic markers and promoted more serious osteolysis, which supported our hypotheses (Fig. 6D and Additional file 7: Fig. S6D). Previously Dyrk1a has been reported to interact with Nfatc1, an osteolytic marker and also a key osteolytic transcription factor, to modulate the bone homeostasis[24]. In addition, inhibition of Dyrk1a accumulated Nfatc1 in the nucleus by reducing its nuclear export [25]. Thus, we speculated whether repression of Dyrk1a by miR-378a-3p enhanced the nuclear translocation of Nfatc1. To investigate this possibility, we performed a coIP assay in RAW264.7 cells and found that the interaction between Dyrk1a and Nfatc1 was impaired after overexpression of miR-378a-3p mimics (Fig. 6E). Moreover, by nuclear and cytoplasmic protein extraction assays, we confirmed reduced expression of Dyrk1a in both the nucleus and cytoplasm but significantly increased nuclear translocation of Nfatc1 (Fig. 6F). Taken together, these results indicate that miR-378a-3p promotes osteolysis for PCa bone metastasis via targeting Dyrk1a to improve the nuclear translocation of the key transcription factor Nfatc1.

MiR-378a-3p induced osteolysis increases secretion of ANGPTL2 to promote PCa progression as a positive feedback loop

Given the fact that mature osteoclasts can promote tumor progression and growth of metastatic nodes in the bone through secretion of soluble factors [26], we herein further investigated whether miR-378a-3p induced osteolysis could facilitate PCa progression in a similar way. To this purpose, we first collected conditioned medium from mature osteoclasts that were either pre-incubated with conEVs (named CM1) vs. 378EVs (named CM2) or pre-overexpressed with control mimics (named CM3) vs. miR-378a-3p mimics (named CM4). Then we treated PC3 cells with these conditioned medium respectively for 3 days (Additional file 8: Fig. S7A). We found that after incubation with either CM2 or CM4, cell proliferation and migration were enhanced compared to relevant controls respectively (Fig. 7A, 7B, Additional file 8: Fig.

S7B and S7C). Furthermore, by mass spectrographic analysis and ELISA assay, we identified a soluble oncogenic protein ANGPTL2 [27] was highly expressed in both CM2 and CM4 (Fig. 7C, Additional file 8: Fig. S7D and Additional file 1:Table S4). Consistently, data analysis from GEO database also revealed a significant physiological upregulation of ANGPTL2 expression in mature osteoclasts (Additional file 8: Fig. S7E). In addition, the expression of ANGPTL2 was positively associated with Gleason Score progression and negatively associated with disease free survival in PCa patients (Additional file 8: Fig. S7F). For further confirmation, we employed an anti-ANGPTL2 antibody to mix with either CM2 or CM4 before placed in PC3 cell cultures. We found that after antibody pre-treatment (Additional file 8: Fig. S7G), the promotional function of both CM2 and CM4 on tumor proliferation and migration was attenuated, which indicated that ANGPTL2 was a main effective factor for the pro-malignant function of CM2 and CM4 (Fig. 7D, 7E, Additional file 8: Fig. S7H and S7I). To investigate the potential mechanism on upregulation of ANGPTL2 expression during miR-378a-3p induced osteolysis, we examined the promoter region of ANGPTL2 and confirmed four Nfatc1 binding sites harbored in this area by ChIP assay, indicating a potential activation by Nfatc1 (Fig. 7F and Additional file 8: Fig. S7J). In addition, application of an Nfatc1 inhibitor (10μg/ml) decreased ANGPTL2 expression in osteoclasts, confirming Nfatc1 as an upstream regulator of ANGPTL2 expression (Additional file 8: Fig. S7K). Thus, all these findings suggest that miR-378a-3p enriched EVs formed a pro-bone metastatic niche by promoting osteolysis and in turn induced an increased expression and secretion of ANGPTL2 for improvement of tumor proliferation and migration as a feedback loop.

Discussion

Growing evidence supported that tumor-derived EVs are key regulators of tumor microenvironment involved in the communication between tumor cells and adjacent bone cells during the process of bone metastasis [28, 29]. In this study, we demonstrated an underlying mechanism by which tumor-derived miR-378a-3p enriched EVs promote osteolysis via the Dyrk1a/Nfatc1 pathway to upregulate the expression and secretion of ANGPTL2 to enhance the proliferation and metastasis of PCa as a positive feedback loop (Fig. 8).

Although miR-378a-3p has been reported as either an oncogenic or tumor suppressive microRNA in different cancers [30–32], we herein observed a tumor suppressive effect of miR-378a-3p on PCa cell proliferation and metastasis when EVs release was inhibited by GW4869. Combined with other findings indicating a lower endogenous concentration of mature miR-378a-3p but a similar one of primary miR-378a-3p precursors in PCa cells vs. BPH cells, we hypothesized that tumor-derived EVs mediated the release of miR-378a-3p for maintenance of the malignant phenotype of PCa cells. As evidence to support for this hypothesis, we identified MAOA, a PCa related oncogene, as a novel target of miR-378a-3p to promote EMT [33]. As a treatment, overexpression of miR-378a-3p along with incubation of GW4869 significantly repressed MAOA expression to inhibit cell proliferation and migration in PC3 cells. On the other hand, we also revealed that upregulated hnRNPA2B1 recruited miR-378a-3p into EVs. Notably, although the relevance between low intracellular concentration of miR-378a-3p and elevated expression of hnRNPA2B1 needed to be further investigated, our findings indicated an alternative therapeutic

strategy for bone-metastatic PCa by exogenous overexpression of miR-378a-3p along with blockage of miR-378a-3p-enriched EV release via inhibiting hnRNPA2B1 expression or its activity.

It is worth mention that although tumor suppressive microRNAs were indicated as tumor metabolic wastes [34], our findings herein demonstrated that miR-378a-3p released from PCa acted as “messenger” from PCa cells to BMMs to form a pro-metastatic niche via promoting osteolysis. On one hand, exocytosis of miR-378a-3p-enriched EVs effectively decreased intracellular concentration of miR-378a-3p to induced the MAOA mediated EMT for tumor metastasis. On the other hand, EV-delivered miR-378a-3p could be absorbed by BMMs to promote pathological osteolysis by targeting the Dyrk1a/Nfatc1 pathway for formatting a pro-metastatic niche. Observation from our in vitro and in vivo investigation provides evidence to support our conclusion that tumor-derived EV-delivered miR-378a-3p is a main factor for promoting pathological osteolysis. First, the particle number of EVs showed no significant difference in either PC3-378OE or PC3-con cells culture medium, but a significant enrichment of miR-378a-3p is confirmed in PC3-378OE derived EVs. Second, both miR-378a-3p-enriched EVs and control EVs exhibit a similar absorption by BMMs. Third, after education with miR-378a-3p-enriched EVs but not control EVs in vivo, more malignant intratibial tumor growth and more serious bone destruction were observed. Consistent with our finding, a study by others also reported a PCa derived EV-delivered miR-152-3p promoted osteolysis via a direct inhibition of Mafb [35]. Thus, combined with other studies together, our findings confirmed that EVs mediated microRNAs transfer plays an important role in the constitution of tumor microenvironment for bone metastasis in PCa.

Increasing studies indicate that during the process of tumor microenvironment remodeling, multiple soluble factors can be secreted from intrinsic cells as a response to the stimulation of tumor [36–39]. In this study, we identified a soluble protein ANGPTL2 that is secreted by mature osteoclasts after educated by miR-378a-3p-enriched EVs. Our study is of particular importance as ANGPTL2 is a homological glycoprotein to the angiopoietins which are members of the VEGF family and is involved in metastasis of multiple cancers [27, 40, 41]. In addition, ANGPTL2 plays an essential role in osteoclast generation by regulating the proliferation and inflammation of osteoclast lineage cells [42]. Therefore, these researches support our observation of upregulated ANGPTL2 expression and secretion in mature osteoclasts as a response to miR-378a-3p induced promotion of osteolysis.

Conclusions

In conclusion, our study demonstrates that miR-378a-3p-enriched EVs drive a positive feedback loop between PCa cells and osteoclasts to format a pro-metastatic niche via promoting osteolysis. Mechanistically, elevated expression of hnRNPA2B1 recruits miR-378a-3p into EVs for release so to promote a MAOA-mediated EMT in PCa cells. Meanwhile, EV-delivered miR-378a-3p accelerates osteolysis and enhances proliferation and metastasis of PCa via targeting the Dyrk1a/Nfatc1 axis to upregulate the expression and secretion of ANGPTL2. These findings indicated that reducing the release of miR-378a-3p-containing EVs or inhibiting the recruitment of miR-378a-3p into EVs might be a potential therapeutic strategy for PCa bone metastasis.

Abbreviations

Abbreviations	Full Names
BMD	Bone Mineral Density
BPH	Benign prostatic hyperplasia
BMMs	Bone marrow macrophages
bmPCa	Bone metastatic prostate cancer
BV/TV	Bone Volume/Tissue Volume
ChIP	Chromatin immune-precipitation
CM	Conditioned Medium
co-IP	Co-immunoprecipitation
DFI	Disease Free Interval
DFS	Disease Free Survival
ELISA	Enzyme-linked immunosorbent assay
EMT	Epithelial-to-mesenchymal transition
ES/BS	Eroded surface per bone surface
EV	Extracellular vesicle
IF	Immunofluorescence
IHC	Immunohistochemical
nbmPCa	Non-bone metastatic prostate cancer
N.Oc/BS	Osteoclast number per bone surface
OS	Overall Survival
PCa	Prostate cancer
RBP	RNA Binding Protein
RIP	RNA Immunoprecipitation
TCGA	The Cancer Genome Atlas
3'UTR	3'Untranslated Region

Declarations

Ethics approval and consent to participate

This study was approved by the Ethics Committee at the Renji Hospital, Shanghai Jiao Tong University School of Medicine, China. All procedures performed in the studies involving human participants were in accordance with the ethical standards of the institutional and with the 1964 Helsinki Declaration and its later amendments or comparable ethical standards. Informed consent was obtained from all individual participants included in the study. All mice were housed and all the mouse experimental procedures were performed according to the protocols approved by the Ren Ji Hospital Medical Experimental Animal Care Commission.

Consent for publication

Not applicable.

Availability of data and materials

The datasets used and analyzed during the current study are available within the manuscript and its additional files.

Competing interests

The authors declare that they have no competing interests.

Funding

This work was supported by the Chinese Ministry of Science and Technology under Grant (2017YFA0102900 to WQG), National Natural Science Foundation of China under Grant (81874097 and 82072843 to YXF; 81630073 and 81872406 to WQG and 81672850 to BD), Science and Technology Commission of Shanghai Municipality under Grant (16JC1405700 to WQG and 19411967400 to BD), High Peak IV subject on stem cells and translational medicine from Education Commission of Shanghai Municipality to WQG; 111 project (B21024) and KC Wong foundation to WQG.

Authors' contributions

JW, YXF, WQG and BD conceived the concept and designed the experiments; JW, XW, XD, HX and JN performed all experiments and data analyses; JW and YXF contributed to original manuscript drafting; JW, YXF, WQG and BD contributed to manuscript editing. All authors read and approved the final manuscript.

Acknowledgements

Not applicable.

References

1. Ganguly SS, Li X, Miranti CK: **The host microenvironment influences prostate cancer invasion, systemic spread, bone colonization, and osteoblastic metastasis.** *Frontiers in oncology* 2014, **4:**364.
2. Brown JE, Cook RJ, Major P, Lipton A, Saad F, Smith M, Lee K-A, Zheng M, Hei Y-J, Coleman RE: **Bone turnover markers as predictors of skeletal complications in prostate cancer, lung cancer, and other solid tumors.** *Journal of the National Cancer Institute* 2005, **97:**59-69.
3. Zhang J, Dai J, Qi Y, Lin DL, Smith P, Strayhorn C, Mizokami A, Fu Z, Westman J, Keller ET: **Osteoprotegerin inhibits prostate cancer-induced osteoclastogenesis and prevents prostate tumor growth in the bone.** *The Journal of clinical investigation* 2001, **107:**1235-1244.
4. Keller ET, Brown J: **Prostate cancer bone metastases promote both osteolytic and osteoblastic activity.** *Journal of cellular biochemistry* 2004, **91:**718-729.
5. Smith MR: **Osteoclast targeted therapy for prostate cancer: bisphosphonates and beyond.** *Urologic oncology* 2008, **26:**420-425.
6. Mathieu M, Martin-Jaular L, Lavieu G, Théry C: **Specificities of secretion and uptake of exosomes and other extracellular vesicles for cell-to-cell communication.** *Nature cell biology* 2019, **21**.
7. Xu R, Rai A, Chen M, Suwakulsiri W, Greening DW, Simpson RJ: **Extracellular vesicles in cancer - implications for future improvements in cancer care.** *Nature reviews Clinical oncology* 2018, **15:**617-638.
8. Joeckel E, Haber T, Prawitt D, Junker K, Hampel C, Thüroff JW, Roos FC, Brenner W: **High calcium concentration in bones promotes bone metastasis in renal cell carcinomas expressing calcium-sensing receptor.** *Molecular cancer* 2014, **13:**42.
9. Wang W, Yang X, Dai J, Lu Y, Zhang J, Keller ET: **Prostate cancer promotes a vicious cycle of bone metastasis progression through inducing osteocytes to secrete GDF15 that stimulates prostate cancer growth and invasion.** *Oncogene* 2019, **38:**4540-4559.
10. Wang Y, Fang Y-X, Dong B, Du X, Wang J, Wang X, Gao W-Q, Xue W: **Discovery of extracellular vesicles derived miR-181a-5p in patient's serum as an indicator for bone-metastatic prostate cancer.** *Theranostics* 2021, **11:**878-892.
11. Ell B, Mercatali L, Ibrahim T, Campbell N, Schwarzenbach H, Pantel K, Amadori D, Kang Y: **Tumor-induced osteoclast miRNA changes as regulators and biomarkers of osteolytic bone metastasis.** *Cancer cell* 2013, **24:**542-556.
12. Fang YX, Zhang XB, Wei W, Liu YW, Chen JZ, Xue JL, Tian L: **Development of chimeric gene regulators for cancer-specific gene therapy with both transcriptional and translational targeting.** *Molecular biotechnology* 2010, **45:**71-81.
13. Kaur G, Ahn J, Hankenson KD, Ashley JW: **Stimulation of Notch Signaling in Mouse Osteoclast Precursors.** *Journal of visualized experiments : JoVE* 2017.
14. Théry C, Witwer KW, Aikawa E, Alcaraz MJ, Anderson JD, Andriantsitohaina R, Antoniou A, Arab T, Archer F, Atkin-Smith GK, et al: **Minimal information for studies of extracellular vesicles 2018 (MISEV2018): a position statement of the International Society for Extracellular Vesicles and update of the MISEV2014 guidelines.** *Journal of extracellular vesicles* 2018, **7:**1535750.

15. Ritchie ME, Phipson B, Wu D, Hu Y, Law CW, Shi W, Smyth GK: **limma powers differential expression analyses for RNA-sequencing and microarray studies.** *Nucleic acids research* 2015, **43:**e47.
16. Jones MP, Crowley J: **A general class of nonparametric tests for survival analysis.** *Biometrics* 1989, **45:**157-170.
17. Chandrashekar DS, Bashel B, Balasubramanya SAH, Creighton CJ, Ponce-Rodriguez I, Chakravarthi BVSK, Varambally S: **UALCAN: A Portal for Facilitating Tumor Subgroup Gene Expression and Survival Analyses.** *Neoplasia (New York, NY)* 2017, **19:**649-658.
18. Li J, Yang X-M, Wang Y-H, Feng M-X, Liu X-J, Zhang Y-L, Huang S, Wu Z, Xue F, Qin W-X, et al: **Monoamine oxidase A suppresses hepatocellular carcinoma metastasis by inhibiting the adrenergic system and its transactivation of EGFR signaling.** *Journal of hepatology* 2014, **60:**1225-1234.
19. Hupkes M, Sotoca AM, Hendriks JM, van Zoelen EJ, Dechering KJ: **MicroRNA miR-378 promotes BMP2-induced osteogenic differentiation of mesenchymal progenitor cells.** *BMC molecular biology* 2014, **15:**1.
20. Huang B, Zhou Z, Liu J, Wu X, Li X, He Q, Zhang P, Tang X: **The role of monoamine oxidase A in HPV-16 E7-induced epithelial-mesenchymal transition and HIF-1α protein accumulation in non-small cell lung cancer cells.** *International journal of biological sciences* 2020, **16:**2692-2703.
21. Villarroya-Beltri C, Baixauli F, Gutiérrez-Vázquez C, Sánchez-Madrid F, Mittelbrunn M: **Sorting it out: regulation of exosome loading.** *Seminars in cancer biology* 2014, **28**.
22. Villarroya-Beltri C, Gutiérrez-Vázquez C, Sánchez-Cabo F, Pérez-Hernández D, Vázquez J, Martin-Cofreces N, Martinez-Herrera DJ, Pascual-Montano A, Mittelbrunn M, Sánchez-Madrid F: **Sumoylated hnRNPA2B1 controls the sorting of miRNAs into exosomes through binding to specific motifs.** *Nature communications* 2013, **4:**2980.
23. Wang M, Xia F, Wei Y, Wei X: **Molecular mechanisms and clinical management of cancer bone metastasis.** *Bone research* 2020, **8:**30.
24. Lee Y, Ha J, Kim HJ, Kim Y-S, Chang E-J, Song W-J, Kim H-H: **Negative feedback Inhibition of NFATc1 by DYRK1A regulates bone homeostasis.** *The Journal of biological chemistry* 2009, **284:**33343-33351.
25. Egusa H, Doi M, Saeki M, Fukuyasu S, Akashi Y, Yokota Y, Yatani H, Kamisaki Y: **The small molecule harmine regulates NFATc1 and Id2 expression in osteoclast progenitor cells.** *Bone* 2011, **49:**264-274.
26. Futakuchi M, Fukamachi K, Suzui M: **Heterogeneity of tumor cells in the bone microenvironment: Mechanisms and therapeutic targets for bone metastasis of prostate or breast cancer.** *Advanced drug delivery reviews* 2016, **99:**206-211.
27. Endo M, Nakano M, Kadomatsu T, Fukuhara S, Kuroda H, Mikami S, Hato T, Aoi J, Horiguchi H, Miyata K, et al: **Tumor cell-derived angiopoietin-like protein ANGPTL2 is a critical driver of metastasis.** *Cancer research* 2012, **72:**1784-1794.
28. Peinado H, Alečković M, Lavotshkin S, Matei I, Costa-Silva B, Moreno-Bueno G, Hergueta-Redondo M, Williams C, García-Santos G, Ghajar C, et al: **Melanoma exosomes educate bone marrow progenitor cells toward a pro-metastatic phenotype through MET.** *Nature medicine* 2012, **18:**883-891.

29. Tamura T, Yoshioka Y, Sakamoto S, Ichikawa T, Ochiya T: **Extracellular Vesicles in Bone Metastasis: Key Players in the Tumor Microenvironment and Promising Therapeutic Targets.** *International journal of molecular sciences* 2020, **21**.
30. Niu F, Dzikiewicz-Krawczyk A, Koerts J, de Jong D, Wijenberg L, Fernandez Hernandez M, Slezak-Prochazka I, Winkle M, Kooistra W, van der Sluis T, et al: **MiR-378a-3p Is Critical for Burkitt Lymphoma Cell Growth.** *Cancers* 2020, **12**.
31. Wang Y, Zhang X, Wang Z, Hu Q, Wu J, Li Y, Ren X, Wu T, Tao X, Chen X, et al: **LncRNA-p23154 promotes the invasion-metastasis potential of oral squamous cell carcinoma by regulating Glut1-mediated glycolysis.** *Cancer letters* 2018, **434:**172-183.
32. Lin Z, Xia S, Liang Y, Ji L, Pan Y, Jiang S, Wan Z, Tao L, Chen J, Lin C, et al: **LXR activation potentiates sorafenib sensitivity in HCC by activating microRNA-378a transcription.** *Theranostics* 2020, **10:**8834-8850.
33. Wu JB, Yin L, Shi C, Li Q, Duan P, Huang J-M, Liu C, Wang F, Lewis M, Wang Y, et al: **MAOA-Dependent Activation of Shh-IL6-RANKL Signaling Network Promotes Prostate Cancer Metastasis by Engaging Tumor-Stromal Cell Interactions.** *Cancer cell* 2017, **31:**368-382.
34. Teng Y, Ren Y, Hu X, Mu J, Samykutty A, Zhuang X, Deng Z, Kumar A, Zhang L, Merchant ML, et al: **MVP-mediated exosomal sorting of miR-193a promotes colon cancer progression.** *Nature communications* 2017, **8:**14448.
35. Ma Q, Liang M, Wu Y, Dou C, Xu J, Dong S, Luo F: **Small extracellular vesicles deliver osteolytic effectors and mediate cancer-induced osteolysis in bone metastatic niche.** *Journal of extracellular vesicles* 2021, **10:**e12068.
36. Coleman RE, Croucher PI, Padhani AR, Clézardin P, Chow E, Fallon M, Guise T, Colangeli S, Capanna R, Costa L: **Bone metastases.** *Nature reviews Disease primers* 2020, **6:**83.
37. Cook LM, Shay G, Araujo A, Aruajo A, Lynch CC: **Integrating new discoveries into the "vicious cycle" paradigm of prostate to bone metastases.** *Cancer metastasis reviews* 2014, **33:**511-525.
38. Fournier PGJ, Juárez P, Jiang G, Clines GA, Niewolna M, Kim HS, Walton HW, Peng XH, Liu Y, Mohammad KS, et al: **The TGF-β Signaling Regulator PMEPA1 Suppresses Prostate Cancer Metastases to Bone.** *Cancer cell* 2015, **27:**809-821.
39. Tang Y, Wu X, Lei W, Pang L, Wan C, Shi Z, Zhao L, Nagy TR, Peng X, Hu J, et al: **TGF-beta1-induced migration of bone mesenchymal stem cells couples bone resorption with formation.** *Nature medicine* 2009, **15:**757-765.
40. Masuda T, Endo M, Yamamoto Y, Odagiri H, Kadomatsu T, Nakamura T, Tanoue H, Ito H, Yugami M, Miyata K, et al: **ANGPTL2 increases bone metastasis of breast cancer cells through enhancing CXCR4 signaling.** *Scientific reports* 2015, **5:**9170.
41. Toiyama Y, Tanaka K, Kitajima T, Shimura T, Kawamura M, Kawamoto A, Okugawa Y, Saigusa S, Hiro J, Inoue Y, et al: **Elevated serum angiopoietin-like protein 2 correlates with the metastatic properties of colorectal cancer: a serum biomarker for early diagnosis and recurrence.** *Clinical cancer research : an official journal of the American Association for Cancer Research* 2014, **20:**6175-6186.

42. Li W-M, Han C-L, Liu C, Xing H-Y, Ding D-C: **ANGPTL2 deletion inhibits osteoclast generation by modulating NF-κB/MAPKs/Cyclin pathways.** *Biochemical and biophysical research communications* 2018, **503:**1471-1477.

Figures

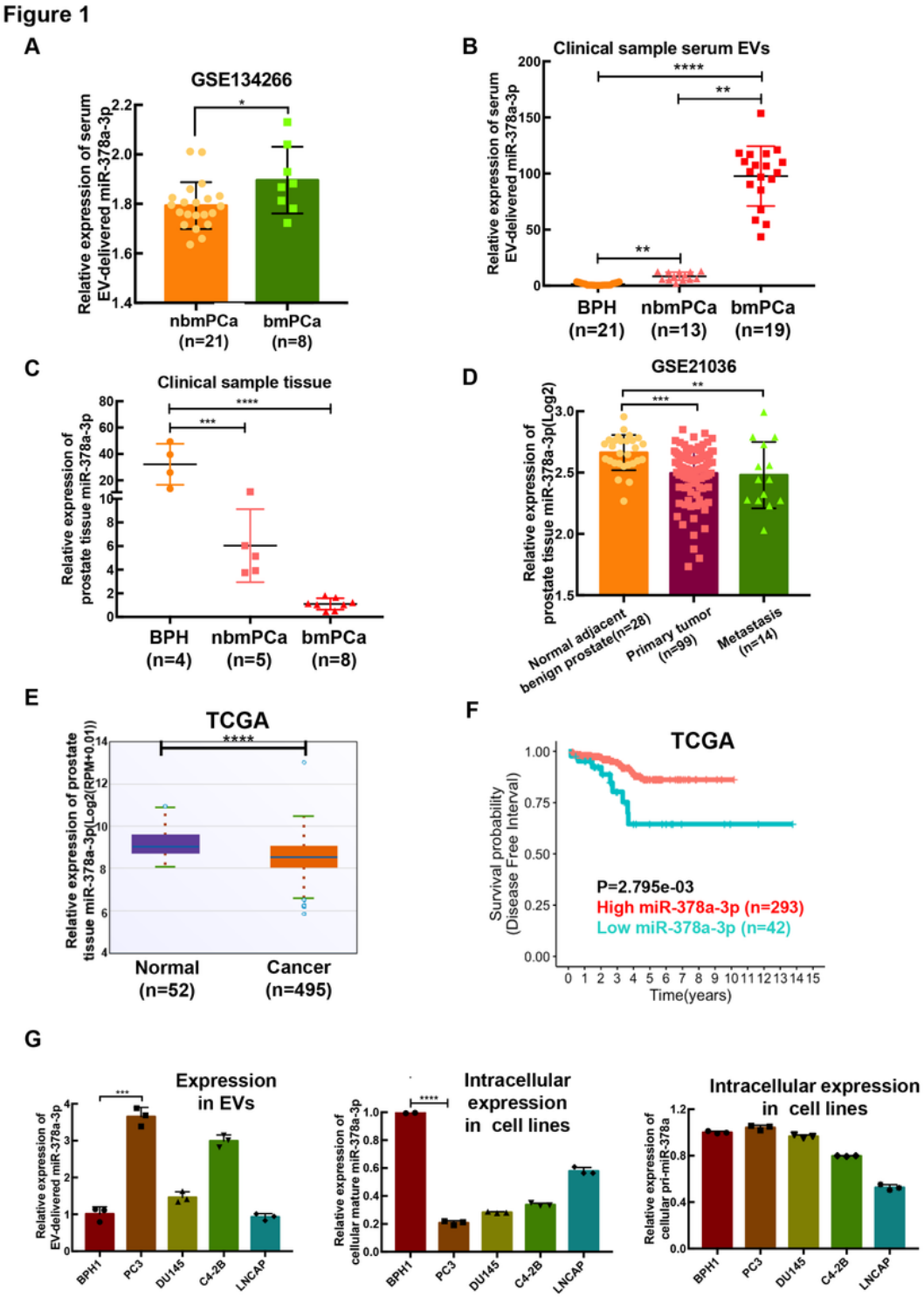

Figure 1

MiR-378a-3p is enriched in bone-metastatic prostate cancer derived EVs. A Upregulated expression of serum EV-delivered miR-378a-3p in bone-metastatic prostate cancer patients by dataset assay from GEO database. B The expression of serum EV-delivered miR-378a-3p is increased in clinical bone-metastatic prostate cancer patients by qRT-PCR assay. C The expression of miR-378a-3p is decreased in clinical tissue samples of bone-metastatic prostate cancer by qRT-PCR assay. D Downregulated expression of miR-378a-3p in clinical tissue samples of bone-metastatic prostate cancer patients by dataset assay from GEO database. E The expression of miR-378a-3p is decreased in clinical tissue samples of prostate cancer patients by dataset assay from TCGA database. F Kaplan–Meier survival analysis revealed a negative relation of miR-378a-3p expression in tissues with disease free interval by dataset assay from TCGA database. G The expression of EV-delivered miR-378a-3p, intracellular mature miR-378a-3p and intracellular pri-miR-378a-3p in BPH-1 cell line and prostate cancer cell lines. BPH: benign prostatic hyperplasia, nbmPCa: non-bone metastatic PCa, bmPCa: bone metastatic PCa. Each bar is the mean value taken from 3 or more independent experiments with error bars indicating standard error. (Asterisks indicate p values as follows:*p < 0.05; **p < 0.01; ***p < 0.001; ****p < 0.0001).

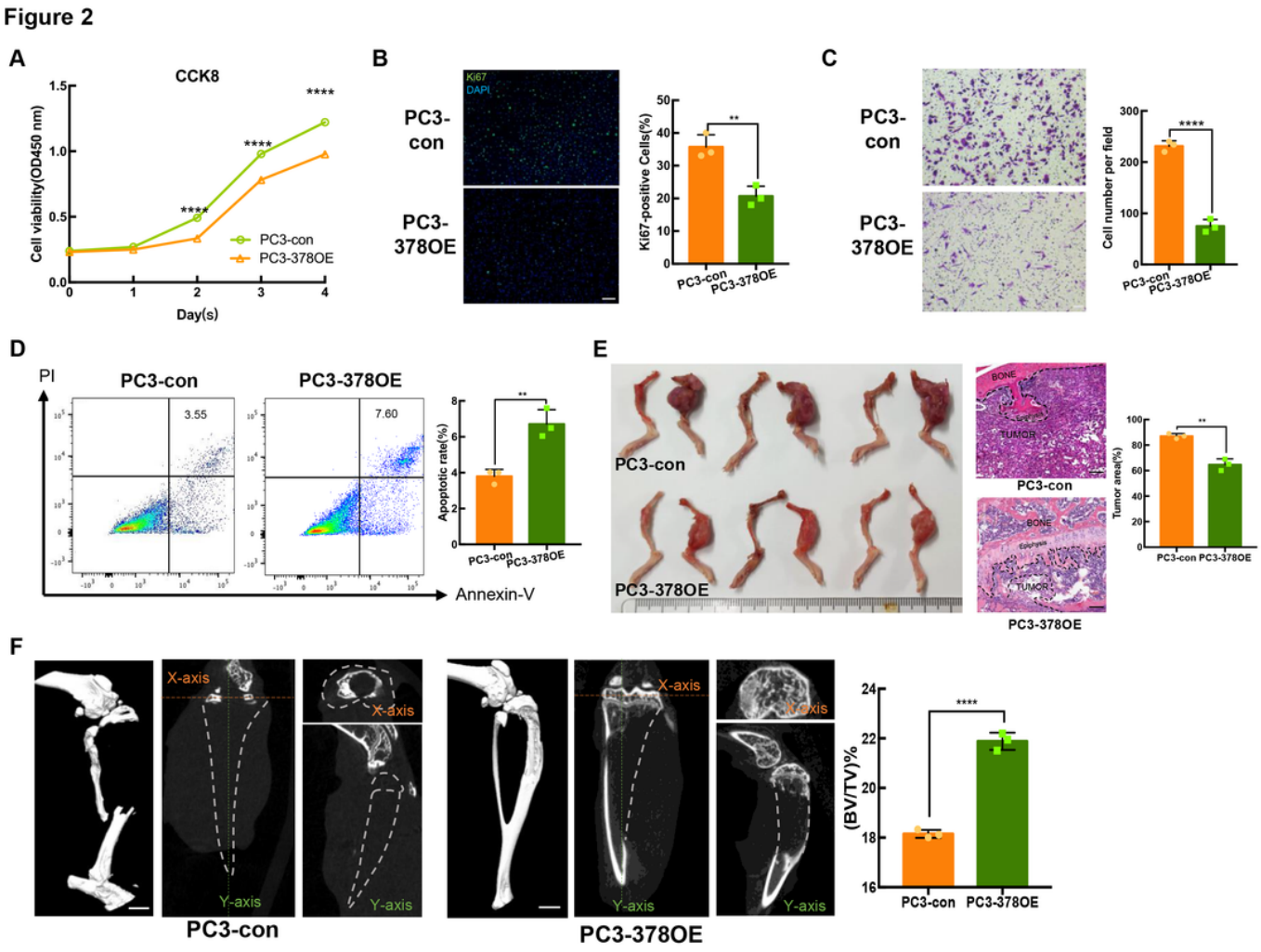

Figure 2

Overexpression of miR-378a-3p with blockage of EVs release inhibits PCa cell proliferation and metastasis. A Cell proliferation assays in PC3-378OE cells compared with PC3-con cells under the condition of GW4869 treatment. B Representative image of Ki67-positive cells in PC3-con and PC3-378OE cells. Bar represents 100 μm C Transwell assays in PC3-378OE cells compared with PC3-con cells under the condition of GW4869 treatment. Bar represents 100 μm D Flow cytometric analysis of apoptosis in PC3-con and PC3-378OE cells. E Overexpression of miR-378a-3p with blockage of EVs release inhibits the growth of intratibial xenograft. Bar represents 200 μm F Representative images of microCT for evaluation of bone destruction in PC3-con group and PC3-378OE group. Bar represents 500mm. Each bar is the mean value taken from 3 or more independent experiments with error bars indicating standard error. (Asterisks indicate p values as follows:**p < 0.01; ****p < 0.0001)

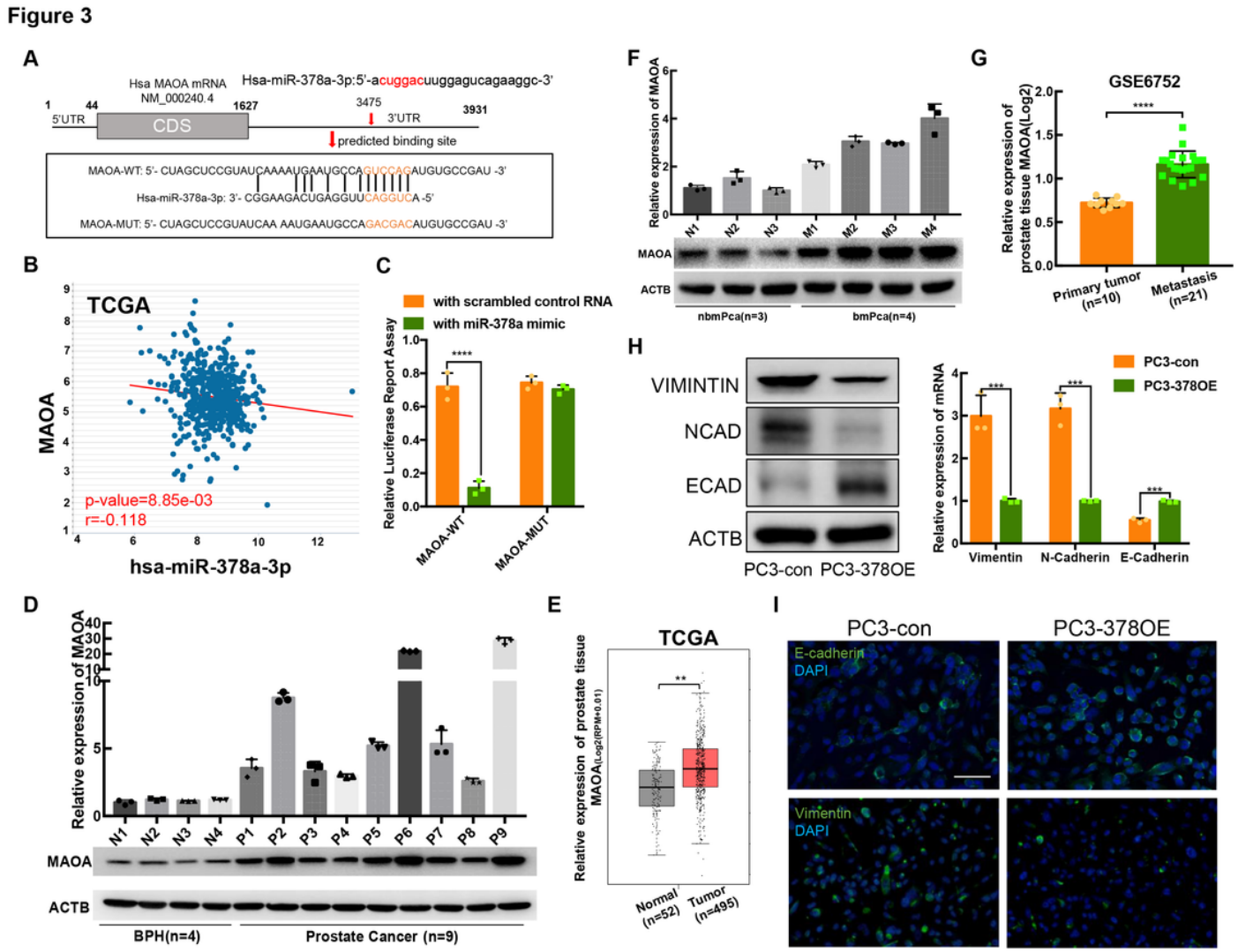

Figure 3

Overexpression of miR-378a-3p inhibits EMT for metastasis in PC3 cells via targeting MAOA. A Predicted binding site of miR-378a-3p in 3'UTR of MAOA mRNA by bioinformatics assay. B Correlation between miR-378a-3p expression and MAOA expression in PCa tissues by data assay from the TCGA dataset. C Identification of miR-378a-3p binding on MAOA mRNA 3'UTR by dual-luciferase reporter assay. D The

expression of MAOA is upregulated in PCa tissues (n=9) compared to BPH tissues (n=4). E The expression of MAOA is upregulated in PCa tissues by data assay from the TCGA dataset. F The expression of MAOA is upregulated in bmPCa (n=4) tissues vs. nbmPCa tissues (n=3). G The expression of MAOA is upregulated in patients with metastatic PCa by data assay from the GSE6752 dataset. H The expression of EMT markers in PC3-con and PC3-378OE cells. I Representative image of E-cadherin and Vimentin IF staining in PC3-con and PC3-378OE cells. Bar represents 50 μm. Each bar is the mean value taken from 3 or more independent experiments with error bars indicating standard error. (Asterisks indicate p values as follows:**p < 0.01; ***p < 0.001; ****p < 0.0001)

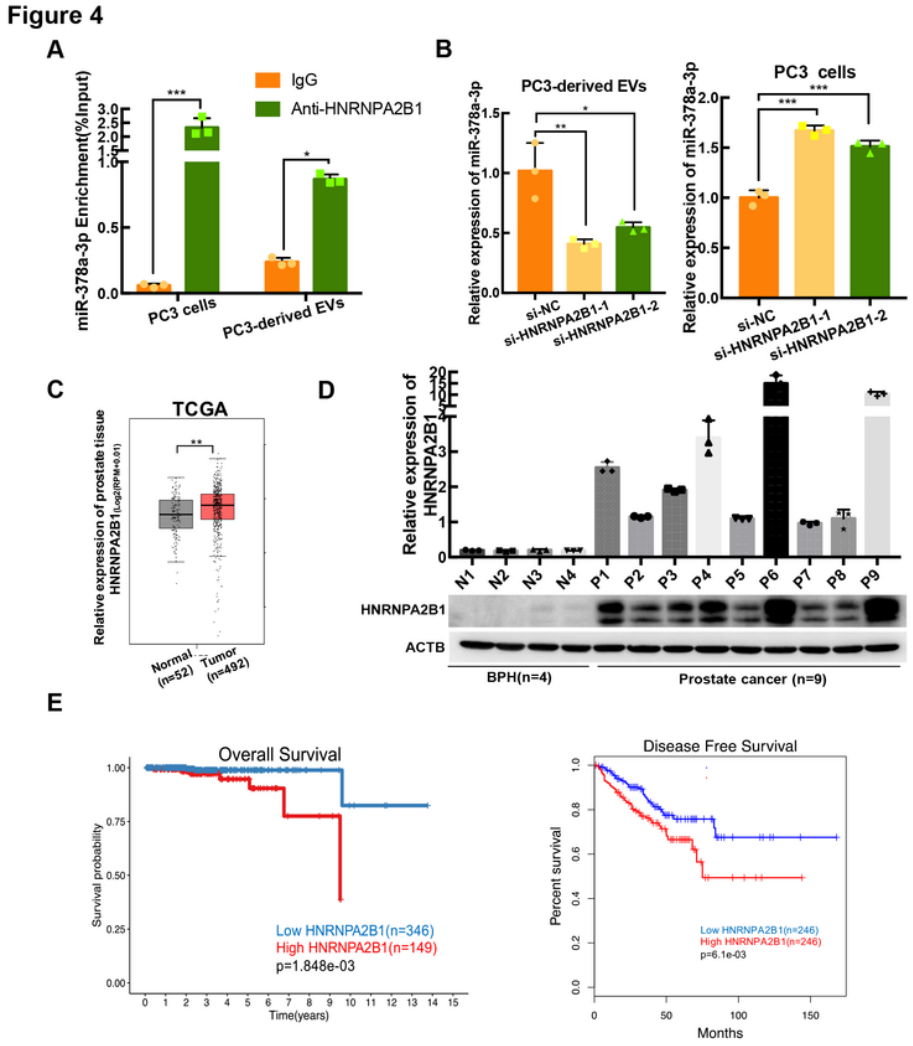

Figure 4

Overexpression of hnRNPA2B1 induced enrichment of miR-378a-3p in tumor released EVs. A RIP assays with anti-hnRNPA2B1 antibody were performed on PC3-cells and PC3-derived EVs. IgG served as the negative control. B The expression of hnRNPA2B1 in PC3-derived EVs and PC3-cells after hnRNPA2B1 knockdown C The expression of hnRNPA2B1 is upregulated in PCa tissues by data assay from the TCGA dataset. D The expression of hnRNPA2B1 is upregulated in PCa tissues (n=9) vs. BPH (n=4). E Kaplan–Meier survival analysis revealed a negative relation of MAOA expression in tissues with overall survival

and disease free survival by data assay from the TCGA dataset. Each bar is the mean value taken from 3 or more independent experiments with error bars indicating standard error. (Asterisks indicate p values as follows:*p < 0.05; **p < 0.01; ***p < 0.001.)

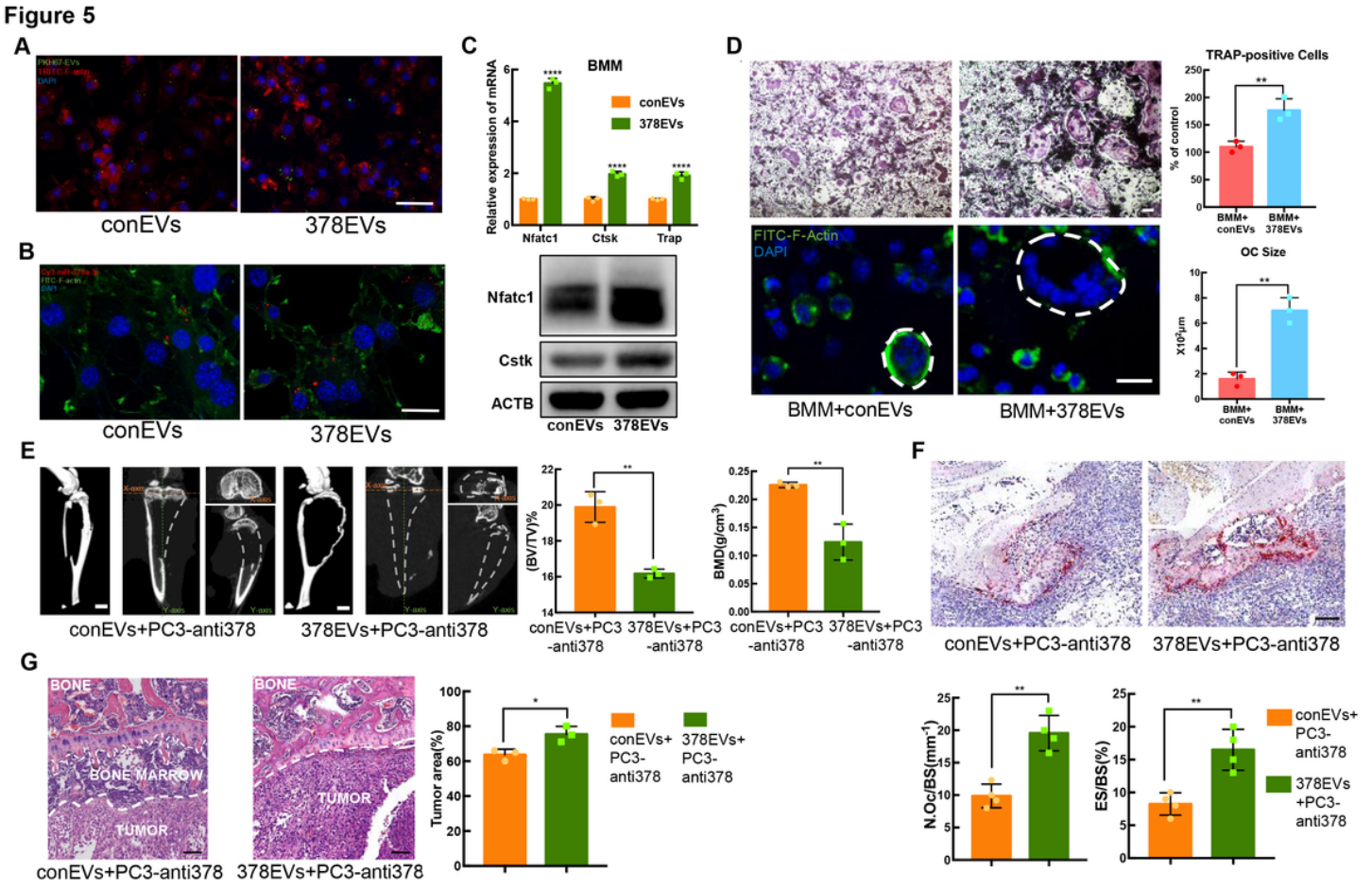

Figure 5

EV-delivered miR-378a-3p promotes osteolytic progression in BMMs. A Representative image of intake of PKH67-labeled EVs by BMMs. Bar represents 50 μm B Representative image of intake of Cy3-labeled miR-378a-3p (red) by BMMs. Bar represents 50 μm C The expression of osteolytic markers is upregulated after incubation of miR-378a-3p enriched EVs. D Representative image of osteolysis by IF actin ring staining and TRAP staining in BMMs incubated with 378EVs vs. conEVs. Bar represents 25 μm. E Representative image of bone destruction after the education of 378EVs or conEVs along with intratibial inoculation of PC3-anti378 cells by microCT. Bar represents 500mm F Representative image of TRAP staining in conEVs+PC3-anti378 group and 378EVs+PC3-anti378 group. Bar represents 200 μm. G Representative image of HE stainging of intratibial xenograft sizes in conEVs+PC3-anti378 group and 378EVs+PC3-anti378 group. Bar represents 200 μm. Each bar is the mean value taken from 3 or more independent

experiments with error bars indicating standard error. (Asterisks indicate p values as follows:*p < 0.05; **p < 0.01; ***p < 0.001; ****p < 0.0001)

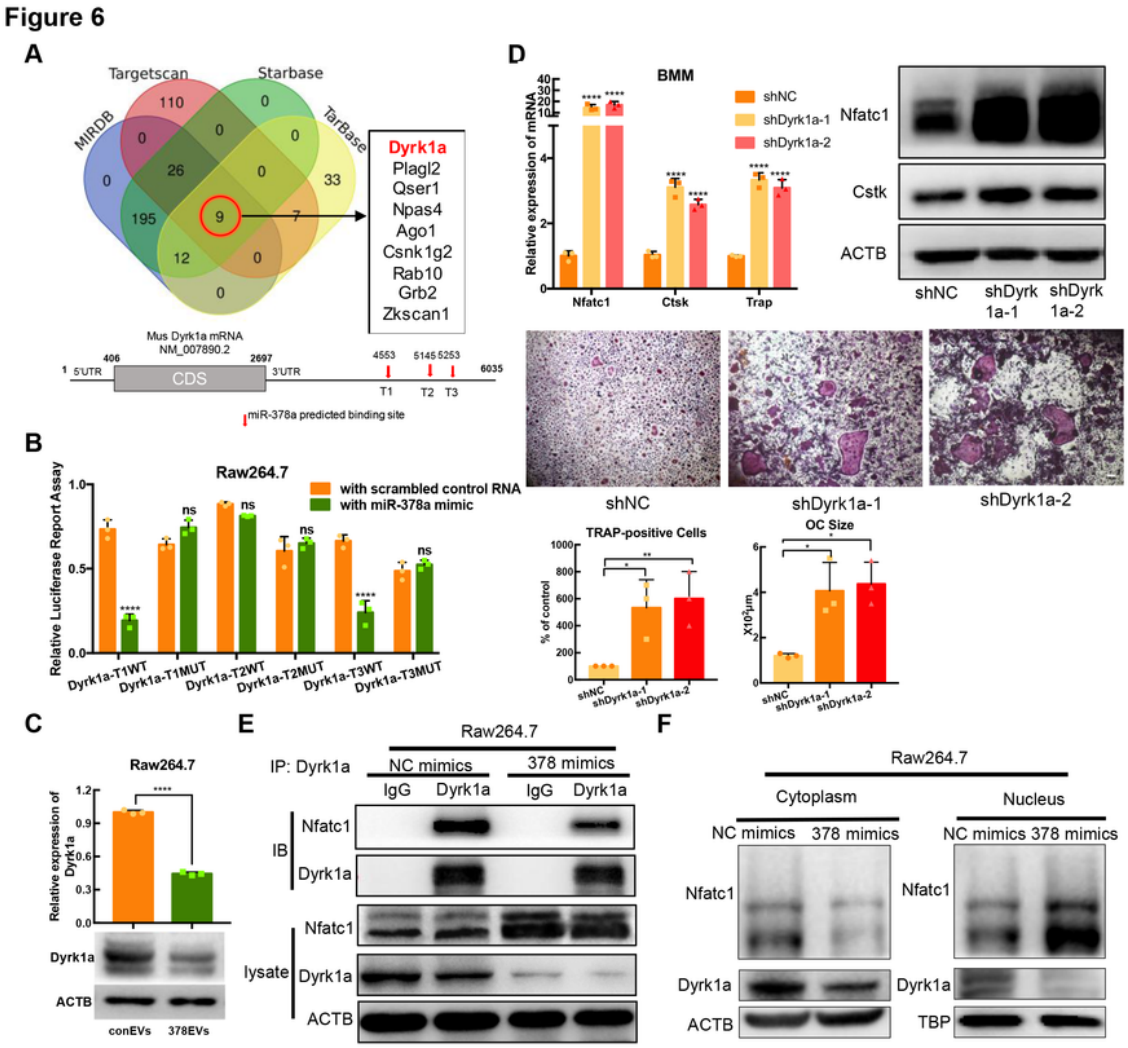

Figure 6

EV-delivered miR-378a-3p promotes osteolysis via targeting Dyrk1a/Nfatc1 signaling pathway. A Predicted binding site of miR-378a-3p in 3'UTR of mouse Dyrk1a mRNA by bioinformatics assay. B Identification of miR-378a-3p binding on mouse Dyrk1a mRNA 3'UTR by dual-luciferase reporter assay. C

Downregulation of Dyrk1a expression after incubation of 378EVs in RAW264.7 cells. D The expression of osteolytic markers was upregulated and TRAP staining was enhanced after knockdown of Dyrk1a by specific shRNAs. Bar represents 100 μm E The interaction of Dyrk1a with Nfatc1 was attenuated after overexpression of 378 mimics in Raw264.7 cells by co-IP assays. IgG served as the negative control. F The nuclear-cytoplasmic translocation of Dyrk1a and Nfatc1 after overexpression of 378 mimics in Raw264.7 cells by western blot assay. Each bar is the mean value taken from 3 or more independent experiments with error bars indicating standard error. (Asterisks indicate p values as follows:*$p < 0.05$;**$p < 0.01$; ****$p < 0.0001$)

Figure 7

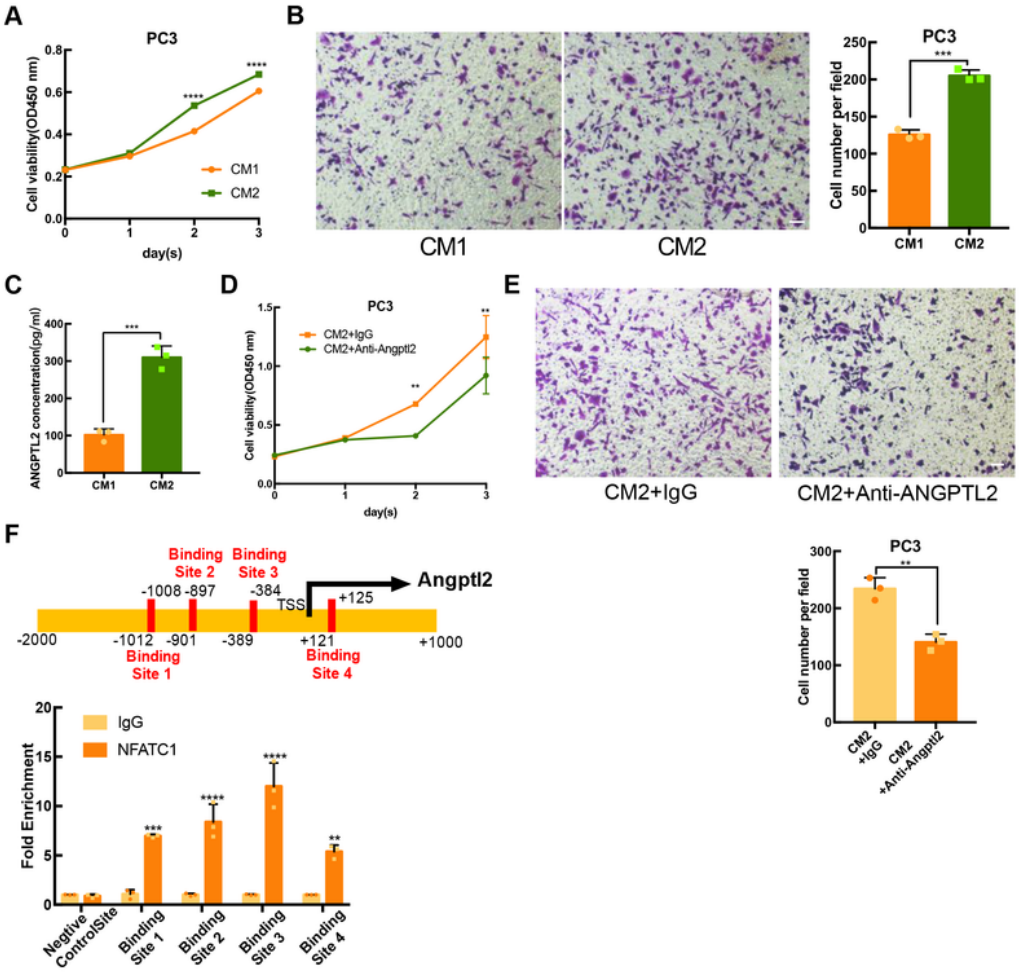

Figure 7

MiR-378a-3p induced osteolysis increased secretion of ANGPTL2 to promote PCa progression. A Cell proliferation assays of PC3 cells after incubation with CM1 or CM2. B The migration of PC3 cells was enhanced after incubation with CM2 by transwell assay. Bar represents 100 μm C The concentration of ANGPTL2 was detected by ELISA in CM1 and CM2. D Cell proliferation assays of PC3 cells after incubation with CM2 combined with IgG or anti- ANGPTL2 antibody. E The migration of PC3 cells was

inhibited after incubation with CM2 combined with anti- ANGPTL2 antibody by transwell assay. Bar represents 100 μm F Identification of Nfatc1 binding sites on ANGPTL2 promoter in Raw264.7 by ChIP assay. Each bar is the mean value taken from 3 or more independent experiments with error bars indicating standard error. (Asterisks indicate p values as follows:**p < 0.01; ***p < 0.001; ****p < 0.0001).

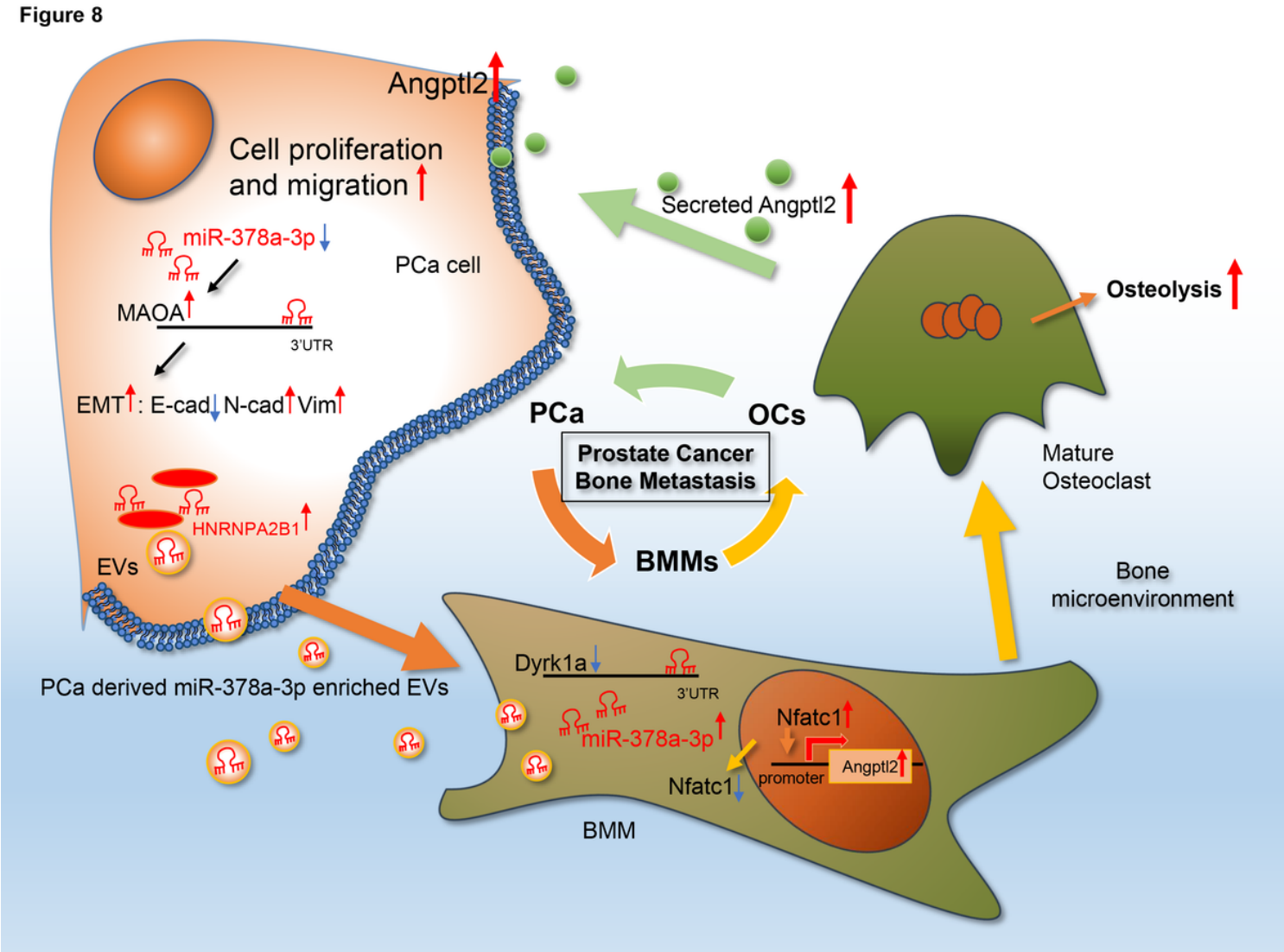

Figure 8

Tumor-derived miR-378a-3p-containing EVs promote osteolysis by activating a Dyrk1a/Nfatc1/Angptl2 axis during tumor bone metastasis. Tumor-derived miR-378a-3p enriched EVs promote osteolysis via the Dyrk1a/Nfatc1 pathway to upregulate the expression and secretion of ANGPTL2 to enhance the proliferation and metastasis of PCa as a positive feedback loop.

Supplementary Files

This is a list of supplementary files associated with this preprint. Click to download.

- Additionalfile1.xls

- Additionalfile2.pdf
- Additionalfile3.pdf
- Additionalfile4.pdf
- Additionalfile5.pdf
- Additionalfile6.pdf
- Additionalfile7.pdf
- Additionalfile8.pdf